Downwind sail aerodynamics: A CFD investigation with high grid resolution

Viola, I.M., Flay, R.G.J.
Sail pressures from full-scale, wind-tunnel and numerical investigations
Ocean Engineering 38 (16) , pp. 1733-1743
DOI: 10.1016/j.oceaneng.2011.08.001

ABSTRACT

The main results of a two-year project aimed at comparing full-scale tests, wind tunnel tests, and numerical analysis predictions are presented. Pressure measurements were obtained from both full-scale tests and wind-tunnel tests, in upwind and downwind conditions. The upwind wind-tunnel test condition was modelled using a Vortex Lattice code, while the downwind wind-tunnel test was modelled using a Navier-Stokes code. The pressures obtained from the three different methods are compared on three horizontal sections of the headsail, mainsail, and asymmetric spinnaker. In general the pressures from the three experiments showed good agreement. In particular, very good agreement was obtained between the numerical computations and the wind tunnel test results. Conversely, the results from the downwind full-scale pressure measurements showed less similarity due to a slightly tightened trim being used for the spinnaker in the on-water tests. Full-scale tests allow the action of unsteadiness due to the wind, wave and yacht movements to affect the results. This unstable environment caused the asymmetric spinnaker to move around, and a tightened trim was required to prevent the spinnaker from collapsing.

INTRODUCTION

Sailing yacht aerodynamics is one of the oldest sciences in the world, but in the last few years it has changed dramatically. For instance, the growth of Computational Fluid Dynamics (CFD) is one of the many examples. Nowadays three-dimensional mathematical models of fully rigged sailplans, and visualisation of the turbulent unsteady flow pattern around them are quite common. Ten years ago such a simulation would have been very rare, and twenty years ago it would have been impossible. In the 1960s, Milgram (Milgram, 1968a, 1968b), Gentry (Gentry, 1971, 1988) and others introduced potential flow codes for solving sail aerodynamics, allowing streamlines to be visualised around sails. In the 1990s, Hedges (Hedges et al., 1996), Miyata (Miyata & Lee, 1999), and others applied Reynolds Averaged Navier-Stokes (RANS) codes to sail aerodynamics, which allowed the separated flow around sails to be visualised for the first time. In the early years of the new millennium, several authors (e.g. Richter et al., 2003, and Renzsch et al., 2008) coupled a finite element structural code with a RANS code, and achieved a so-called *virtual wind tunnel*. The mechanical properties of the sails were modelled and the displacements were computed by the structural code, while the RANS code computed the pressure distributions. The present authors believe that in future years, Large Eddy Simulations (LES) and Detached Eddy Simulations (DES) techniques will commonly be used in sail aerodynamics.

CFD is not the only revolution in sail aerodynamics. Wind tunnel tests have also evolved significantly. In 1994 the Yacht Research Unit (YRU) of the University of Auckland introduced the Twisted Flow Wind Tunnel (Flay, 1996), and significantly increased the agreement between wind-tunnel results and full-scale observations. Before 1994, downwind sails had to be trimmed differently in the existing straight flow wind tunnels from the full-scale trim. This was because the vertical profile of the apparent wind direction was not modelled and a uniform apparent wind direction was used. In fact the apparent wind angle (AWA) is higher at the top of the sail than at the bottom of the sail because of the velocity profile of the true wind. A few years later, three twisted flow devices were introduced into wind tunnels in Europe: at the Politecnico di Milano Wind Tunnel (Zasso et al., 2005), at the Kiel

Yacht Research Unit (Graf & Mueller, 2005), and at the wind tunnel used by BMW Oracle Racing, challenger for the 32nd America's Cup in Valencia.

In 2003 the YRU introduced the Real-Time Velocity Prediction Program (VPP) for wind tunnel testing (Hansen et al., 2003). Nowadays it is estimated that the YRU performs more than 2/3rds of the wind tunnel tests in the world on yacht sails, and it performs only a few of them without using the real-time VPP. In fact, it allows testing in a *free-to-heel condition,* where the hydrodynamic righting moment is computed by the VPP and the associated heel is mechanically applied in real time. In 2006, the Politecnico di Milano Wind Tunnel built a real-time VPP (Fossati et al., 2006). The BMW Oracle wind tunnel was also equipped with a real-time VPP. However, that wind tunnel was dismantled at the end of the 32nd America's Cup.

Sail shape detection was a new milestone in wind tunnel testing. The three twisted flow wind tunnels in Auckland, Kiel and Milan, have all introduced flying shape detection systems over the last five years. Every sail trim is recorded and used to correlate measured overall forces with sail shapes. Three-dimensional mathematical models are also used to perform CFD analysis on the recorded sail shapes. One such investigation, performed at the Politecnico di Milano Wind Tunnel, presented wind tunnel tests systematically modelled with CFD in order to support the sail design process for the Luna Rossa challenger of the 32nd America's Cup (Viola, 2009).

In wind tunnel testing, it is common practice to measure aerodynamic forces on sails, rigging and hull with a 6-component balance placed inside or underneath the yacht model. Even though there are significant interactions among the rig, hull and sails, the rig – hull - sails interaction is automatically taken into account when the real-time VPP is used, as it requires the overall aerodynamic forces, including those on the rig and hull, as well as the sails.

Since wind tunnel tests are increasingly being used to validate CFD simulations, the pressure distribution on the sails, instead of the aerodynamic forces, should be measured. This is because the same aerodynamic force can be achieved by different pressure distributions. Therefore, the computed aerodynamic force might be in agreement with the measured wind-tunnel force, while the numerical and measured pressure fields were in complete disagreement. In the last four years, the YRU has put a great deal of effort into pressure measurements. A pressure system capable of acquiring up to 512 channels at high frequency (details in §3.1) has been developed. Pressures have been measured on both upwind and downwind sails, thus providing an accurate benchmark for CFD analysis. The authors believe that in the near future, pressure measurements and flow visualization techniques will become standard practice in wind tunnel tests.

Full-scale tests have been performed only rarely. Warner & Ober, 1925, performed the first milestone measurements between 1915 and 1921, where U-tube manometers were used to measure pressures on an S-class yacht. In the 1990s, several authors (Milgram et al., 1993; Masuyama & Fusawa, 1997; Hochkirch & Brandt, 1999) measured aerodynamic forces through complex dynamometric frameworks, which connected the rigging to the rest of the yacht. In the past five years, the focus has moved to pressure measurements. Puddu et al, 2006, measured the first complete pressure distributions on a Tornado mainsail. Viola & Flay, 2010a, measured the first pressure distributions on a headsail, and Viola & Flay, 2009, 2010b, measured the first pressure distributions on a downwind sail.

More detailed descriptions on the state of the art of sail aerodynamics can be found in the following papers:

- Viola, 2009:
  Reviews CFD applications in sail aerodynamics

- Viola & Flay, 2009:
  Reviews wind tunnel force measurements on downwind sails

- Viola & Flay, 2010b:
  Reviews pressure measurements on sails performed on-the-water and in the wind tunnel

- Viola & Flay, 2010c:
  Reviews full-scale force and pressure measurements.

The above overview on recent developments in sail aerodynamics shows that new techniques have revolutionised sail aerodynamics. The present authors have been pioneers in applying some of these techniques to sail aerodynamics. This paper presents a comparison between the three measurement approaches. In the last two years, the authors have investigated the pressures on sails with the aim of comparing the three methods: full-scale testing, wind-tunnel testing, and numerical analysis. This paper is a summary of the research results to date. In particular, pressures measured and computed with the three methods are compared in both upwind and downwind conditions. Most of the pressure distributions and the CFD results are presented for the first time in this paper. However, additional results and detailed descriptions of each set of tests have been published in previous papers as summarised in Table 1.

FULL SCALE TESTS

Upwind

On-water tests can be very meaningful in the upwind sailing condition. Small changes in the sail trim and in the sailed course lead to pressure differences that can be measured with high accuracy. Tests were performed on a Sparkman & Stephens 24-foot yacht in the Hauraki Gulf (Auckland, NZ) in breeze of about 4 m/s. Pressures were measured by 6, 9 and 16 pressure taps placed on horizontal sections at ¼, ½ and ¾ of the height of the headsail and mainsail respectively. Figure 1 (left) shows the sailplane of the S&S 24-foot yacht *Aurelie* and the measured sections.

The pressure taps were 1 mm diameter holes at the centre of thin plastic frustums with a base diameter of 20 mm, and a height of 5 mm. Static pressure taps were thus not flush mounted. In a previous study, Flay and Millar (2006) tested this type of pressure tap against standard hole taps. They found frustum-type pressure taps to read about 10% lower pressures than hole-type pressure taps due to local flow acceleration. In the present tests, in order to minimise the local flow acceleration and to reduce this error, tape was used to chamfer the frustum with the sail to make a smoother contour.

The pressure tap in the plastic frustum was connected to a stainless steel tube lying flat against the sail. Pressures were transmitted through 1-mm-bore PVC pressure tubes connected to the steel tubes and to the pressure transducers inside the cabin. The transducers have a pressure range of ±450 Pa and a resolution of 9.25 mV/Pa with an accuracy better than ±0.5 Pa. Additional details are provided by Viola et al., 2010c. The acquisition system could acquire up to 512 channels at 3,900 Hz. Long tubes are known to damp high frequency fluctuations and thus pressures were acquired at 100 Hz and were averaged over 120 seconds. The same pressure system was used in all of the pressure measurements

presented in the present paper. Leeward and windward pressures were measured on starboard and port tacks respectively as the pressure taps were concentrated on the port side of the sail.

The reference static pressure p_∞ was measured inside the yacht cabin. The dynamic pressure q_∞ was measured with Pitot-static tubes fixed onto a pole attached to the stern of the yacht. Subsequent analysis showed that the dynamic pressure measured at this location was about 20% higher than the dynamic pressure at the reference height. The corrected dynamic pressure is used in the analysis and figures herein. In order to compute the pressure coefficient, *Cp*, the static pressure measured inside the cabin p_∞ and the dynamic pressure q_∞ measured on the pole were used. Measurements performed when the yacht was at the wharf showed that the static pressure inside the cabin was a good approximation of the time-averaged static pressure on the poled Pitot-static tubes. Therefore, no corrections were applied to take into account the fact that the reference static and dynamic pressures were measured on different streamlines.

Pressure distributions on the two sails were measured for different sail trims and courses sailed. Several combinations of AoA of the two sails were tested, leading to different gaps between the sails. Several mainsail twists and cambers were tested by trimming the boom vang and the backstay. Small trim or course changes resulted in significantly different pressure distributions. The *Cp* presented herewith were measured at AWA=30° when the sails were trimmed to maximise the boat speed.

Nowadays, a few top sailing teams have tried to measure the sail pressure distributions to optimise the sail trim. However, difficulties have been found in using the measured pressure distributions to optimise the trim or the sailed course (JB Braun, private communications 2010). In fact, to find the optimum pressure distribution, the position of the sails and the hydrodynamic forces must be taken into account. Aerodynamic forces can be computed knowing the pressure distribution and the flying shape geometry simultaneously. The optimum aerodynamic forces can then be computed using a VPP, which computes the aerodynamic-hydrodynamic balance. Nonetheless, the present paper and the other papers in Table 1 show that a full understanding of the pressure distribution trends allows sail trim enhancements, even when the flying shape of the sail and the yacht hydrodynamics are unknown.

Downwind

An asymmetric spinnaker designed for the AC33-class was built by North Sails (NZ) Ltd at 1/3rd scale so that it could be flown on a Platu25-class yacht (the 2&S 24 no longer being available). Pressure taps were embedded into the sail along three horizontal sections. The pressure taps were larger, but similar in design to the taps used in the full-scale upwind tests. 21 1-mm diameter pressure taps, at the centre of 50 mm diameter and 5 mm high frustums were used along each section. 1-mm bore PVC pressure tubes contained in a sleeve in the sail were used to convey the pressures from the taps to the sail tack, and then to the pressure transducers located inside the yacht cabin. The pressures on the leeward and windward sides were measured by sailing on the port and starboard tacks respectively as the pressure taps were concentrated on the starboard side of the sail. The static and the dynamic reference pressures were measured as for the upwind full-scale tests described above. The pressure measurements were acquired at 100 Hz and averaged over 90 seconds. The tests were performed in the Hauraki Gulf (Auckland, NZ) and the dynamic pressure q_∞ varied between 4 Pa and 40 Pa for the tests.

Figure 2 (left) shows a photograph of the yacht and sails set up for the on-water tests, except that the mainsail was reefed slightly in order to align the top of the spinnaker and mainsail to the same height. Measurements were obtained for several sail trims and several courses. The *Cp* presented herewith were measured with the reefed mainsail at AWA=80°, when the sails were trimmed to maximise the

boat speed.

It was observed that the apparent wind direction and speed oscillations were larger when sailing downwind than upwind. This is as expected, as the boat speed subtracts from the wind speed making a lower apparent wind speed, and thus the ratio of the fluctuations in wind speed due to gusts to the mean apparent wind speed is higher in the downwind situation compared to upwind. Moreover, the wind oscillations forced the helmsman to correct the sailed course. Therefore, the sails were trimmed continuously to account the wind and course variations.

WIND-TUNNEL TESTS

Upwind

Wind tunnel tests were performed in the Yacht Research Unit twisted flow wind tunnel on 1/15th-scale model sails of an AC33-class yacht. Pressures were measured on four sections of both the headsail and mainsail. Figure 1 (right) shows the locations of the four sections. In order to compare the wind-tunnel and full-scale tests, the *Cp* presented herewith were measured on the three lowest sections of the headsail and mainsail. The sails were built in fibreglass using a sandwich structure. The core of the sandwich was extruded polypropylene made of parallel square hollow tubes (coreflute), which were used to carry the pressure signals from the measurement locations to the sail foot. 1-mm bore tubes were connected to the foot of the sail and carried the pressures to the pressure transducers. The same pressure system was used for both the full-scale tests and the wind tunnel tests. Thin wires suspended the sails from rigid supports, and a flat plate was used to model the hull deck. Several headsail and mainsail trims were tested for a constant AWA of 19°. The rigid sails and the wire support setup allowed the flying shape of each trim to be measured. Both leeward and windward pressures were measured on port tack.

The reference static pressure p_∞ was measured by a Pitot-static tube located about 10 m upstream of the sails. The tests were performed in nominally uniform flow (without the twisted vane device) and the sails were raised above the floor of the test section and hence were not affected by the wind tunnel boundary layer. The reference dynamic pressure q_∞ was about 32.5 Pa for the tests. Pressures were acquired at 100 Hz and averaged over 90 seconds.

The same sails had been tested previously with a different setup, where they were fixed onto a model-scale rigged yacht. The model was attached to a 6-component balance located under the floor of the wind tunnel, which allowed the aerodynamic forces to be measured. The sails were trimmed to achieve the maximum drive force. The sail trim was recorded and used as the reference sail trim for the subsequent test with the sails supported by the wires. In the present paper, only the *Cp* measured using the wired support setup with the reference sail trim are presented.

Downwind

Three AC33-class asymmetric spinnakers were tested (Figure 2, right). Frustum pressure taps with a squared base 20 mm x 10 mm and 4 mm in height were used in the upwind full-scale tests. These were on the opposite side of the sail to that under investigation, and a 1 mm diameter hole was made in the sail to allow pressure transmission to the tap, resulting in no modification to the local pressure coefficient due to the pressure tap itself. 11 pressure taps were placed on each of five horizontal sections at heights of 1/8, 1/4, 1/2, 3/4, and 7/8 up the spinnaker and mainsail. Conventional flexible sails were used and the pressure taps were glued onto the sails. 1-mm bore PVC pressure tubes, suspended from the mast, connected the taps to the pressure transducers inside the yacht model

cockpit. Pressures were measured at 100 Hz and averaged over 70 seconds, a period long enough to capture stable average values of the pressure signals. The reference static and dynamic pressures were measured as for the upwind wind tunnel tests. The downwind tests were performed at a dynamic pressure of about 6.3 Pa.

The model was attached to a 6-component balance underneath the wind tunnel floor. Forces and moments were measured at 200 Hz and averaged over 70 seconds. Three different asymmetric spinnakers were tested at several AWA, trims, and heel angles. The yacht model was mounted in a trough (300 mm x 1500 mm) filled with water sunk into the wind tunnel floor, which prevented air from passing under the hull. The model yacht and sails were thus subjected to the wind tunnel boundary layer. Tests were performed both with and without the twisted flow device upstream of the model. The pressures discussed below were measured in uniform flow with the flow twisting device removed.

The *Cp* presented herewith were measured at AWA=55° on one of the spinnakers along the three horizontal sections at 1/4, 1/2 and 3/4 of the sail height. The sails were trimmed to maximise the drive force, which was measured with the balance. In this configuration, the windward pressure was measured only along the mid-height section. Further details showing drive force variation with trim are available in Viola and Flay, 2009.

NUMERICAL SIMULATIONS

Upwind

A Vortex Lattice code was used to determine the sail pressure distributions for upwind sailing conditions, when it could be assumed that there was little or no flow separation, while a fully viscous Navier-Stokes code was used for downwind conditions, where there is normally significant flow separation. The inviscid code was developed by Julien Pilate, a research assistant at the Yacht Research Unit, who also ran these simulations. The code was based on the work of Werner, 2001, but was completely rewritten in Matlab. The Kutta condition is employed to close the system. The finite velocity is imposed by setting the strength of the vortex lines at the trailing edge to be equal to 0. Each sail was modelled by 29 by 29 panels with full cosine spacing in both the span-wise and chord-wise directions. A mirror image of the sails was used to make the water surface a plane of symmetry. The vortex lattice code was used to model the wind tunnel test configuration with the sails set at their optimum trim.

The numerical computations give the highest repeatability of the three methods. Unfortunately, it is much more difficult to find the optimum sail trim using a numerical simulation than from conducting a wind tunnel test.

Downwind

The wind tunnel test configuration discussed above was modelled with the Navier-Stokes solver Star-CCM+ 5.04.004 (CD-adapco). The flying shapes of the spinnaker and mainsail in the wind tunnel were detected using photogrammetric techniques, and then sails with these shapes were modelled with zero thickness. The elliptic shapes of the mast and the boom were modelled as zero thickness flat plates in the direction of their maximum diameter. The hull was modelled without taking into account the cockpit recess.

Figure 3 shows the computational domain made of prisms aligned with the boat heading direction. The

wind tunnel floor and roof were modelled by the top and bottom surfaces (in blue in Figure 3) of the prism respectively, where symmetry conditions were applied, in order to model the impermeability of the surfaces. Thus the wind tunnel boundary layer was not modelled. In fact, modelling the wind tunnel boundary layer correctly would have required a very large number of cells because the floor had a large surface (6*L*x6*L*, where *L*=2.3m is the model height) compared to the surface of the yacht model. If low grid resolution were used to model the boundary layer, its thickness would increase excessively, and lead to a larger error than simply neglecting the boundary layer, as was done for the present simulation.

An inflow boundary condition was used on two vertical faces of the prism (left and bottom red faces in Figure 3). A uniform inflow velocity at 55° to the yacht heading was used. A zero turbulent viscosity ratio (ratio of turbulent viscosity to dynamic viscosity) was used at the inlet. In fact, the low grid resolution upstream of the yacht model tends to exaggerate the turbulent viscosity ratio and, therefore, a lower turbulent viscosity ratio was used than the one measured in the wind tunnel. A constant pressure p_∞=0 Pa was imposed on the outflow surfaces (top and right green faces in Figure 3).

The grid was developed within Star-CCM+ with a *trimmed* technique. Hexahedral cells were used and refinement was performed with hanging nodes. The hexahedra were then trimmed to take into account the sail and hull shapes. Figure 4 shows the grid resolution on the model. 1.5 million cells were used.

The steady incompressible Navier-Stokes equations were solved with a segregated approach and second order accuracy. The *k-ε realizable* turbulence model with *two-layer all y+* wall treatment was used. The *all y+* formulation switches from the traditional wall-function approach to the traditional low-Reynolds number approach using a blending function, which is a function of the Reynolds number based on the wall distance. The *two-layer* formulation for the *k-ε realizable* turbulent model switches to a one-equation model in the near-wall region, which solves k but prescribes ε algebraically as a function of the wall distance (Rodi, 1991).

The grids were developed, and the simulations were performed, on the CILEA cluster in Milan (Italy) and were remotely managed from Newcastle University in Newcastle upon Tyne (UK) using the PBS-Professional (Altair Inc.) workload system. The cluster, named Lagrange, is made up of 208 2-ways nodes Intel Xeon 3.16 GHz QuadCore with 16 GB per node, running Red Hat Enterprise Linux Server (Release 5.1) OS. The grid was developed on a serial processor, while the simulations were performed on a 4-core parallel processor.

RESULTS AND DISCUSSION

General Results

Figure 5 shows the general pressure distribution on the headsail, mainsail and asymmetric spinnaker. The pressure coefficient, *Cp*, (see Eq. (1) is defined as the difference between the pressure p and the free-stream static pressure p_∞, normalised by the free-stream dynamic pressure q_∞.

$$Cp=(p- p_\infty)/ q_\infty \quad (1)$$

The headsail and the spinnaker have thin leading edges and, therefore, leading edge separation occurs at angles of attack (AoA) higher than the ideal AoA, i.e. when the flow velocity is tangent to the sail at the leading edge, Note that the ideal AoA is a geometric condition (based on thin aerofoil theory) and trimming the sail at the ideal AoA does not imply achieving optimum performance. There is laminar to

turbulent transition, and then the separated turbulent shear layer reattaches, forming a thin bubble with a high inner velocity. The adverse (positive) pressure gradient following the maximum camber of the sail can lead to trailing edge separation. If it occurs, the pressure recovery is interrupted and the pressure is equal to the so-called *base pressure* up to the end of the profile.

On the mainsail, the bluff-body-shaped mast causes separation of the boundary layer, forming a different kind of leading edge bubble. In contrast to the thin leading edge bubble on the headsail and spinnaker, transition occurs in the after part of the mast bubble, leading to a less energetic reattached boundary layer. The recirculation flow has lower speed and, thus, the resulting leading edge suction peak is smoother (Wilkinson, 1984).

Upwind

Figure 6 shows *Cp* on three sections of the headsail and mainsail. In particular, *Cp* measured in full scale, when the sails were trimmed to maximise the boat velocity, are compared with *Cp* measured in the wind tunnel and computed numerically for the trim that allowed the maximum drive force. Because the pressure distributions on the headsail changed significantly with small variations in the angle of attack, *Cp* for 2 headsail trims measured in full scale are presented: a slightly eased trim where the windward tell-tails were pointing up (named "FS-eased" in Figure 6), and a slightly tightened trim where the tell-tails were horizontal (named "FS-tight"). The two trims (as shown by the tell-tails) are known by good sailors to be optimum trims in different conditions. For instance, while the first trim results in a higher lift/drag ratio, the second trim gives a higher drive force. The pressure on the windward side of the sails is not affected by small changes in the sail trim and, therefore, windward pressure distributions are shown for only one trim.

The *Cp* measured with the 3 methods show that the headsail is trimmed near to the ideal AoA. In fact, the full-scale trim "FS-eased" presents negative leading edge pressure, which shows that the headsail was trimmed at an AoA slightly lower than the ideal AoA, and it was thus close to collapse. Conversely, the "FS-tight" trim presents a large suction peak on the leeward side of the leading edge, which shows that it was trimmed at an AoA slightly higher than the ideal AoA. The *Cp* curves resulting from the optimum trim measured in the wind tunnel and computed numerically lie between the two *Cp* curves measured in full scale, where the full-scale sails were trimmed at two optimum trims for different sailing conditions.

In the tighter full-scale trim ("FS-tight"), on the leeward side of the headsail trailing edge separation occurs, which is indicated by the pressure plateau in the last 40% of the sail girth at the mid-section. If a pressure plateau occurs when the sail is trimmed at an AoA slightly higher than the ideal AoA, then the sail shape can be improved in order to decrease the positive pressure gradients near the trailing edge. For instance, if the maximum camber were further upstream in the mid and top sections of the tested headsail, trailing edge separation would not be expected to occur, and higher suctions would be achieved. The more efficient headsail shape tested in the wind tunnel allowed trailing edge separation to be avoided.

On the mainsail, *Cp* measured with the 3 methods are in relatively good agreement. The small differences can be explained by the different sail shapes, and due to the presence of the mast, which was not present in the model of the sails in the wind tunnel tests and in the numerical simulations. Due to the absence of the mast and the negligible thickness of the mainsail, a leading edge bubble similar to the bubble at the leading edge of the headsail occurs in the wind tunnel flow. The inviscid numerical code was not able to compute such a separation. It is believed that the differences in the pressure

recovery on the leeward side of the mainsail near the leading edge are due to the absence of the leading edge bubble in the numerical simulation.

The suction on the mainsail is significantly lower than that on the headsail due to the downwash effect. Figure 7 shows the streamlines (which are also pathlines) around a horizontal section of a headsail and mainsail computed using a steady 2D Navier-Stokes simulation. Horizontal sections of the headsail (left) and the mainsail (right) are shown in black. Solid streamlines show the trajectories of the air particles (moving from left to right), while the dotted streamlines show the trajectories of the air particles in the absence of a headsail. Figure 7 shows that the presence of the headsail leads to a significant decrease in the leading edge AoA of the mainsail (downwash). Conversely, the leading edge AoA of the headsail would have been smaller if the mainsail were not present (upwash).

It should be noted that while the AWA of the full-scale and wind-tunnel tests are quite different (19° and 30° respectively), the sail trims and the resulting AoA are quite similar. In fact, in the wind tunnel test, the sails were trimmed to maximise the drive force. In the full-scale test, the sails were trimmed to maximise the boat velocity. The two different aims led to very similar trims in the medium/light wind conditions when the full-scale tests were performed. It can be seen from the full-scale tests, the wind-tunnel tests and the numerical simulations, that the similarities in the *Cp* trends on all 3 sections show that the sail had an appropriate twist distribution.

Wind-tunnel tests clearly allow much higher repeatability than full-scale tests, due to the stationarity of the flow. Moreover, pressures and aerodynamic forces can be measured simultaneously. However, these results show that full-scale pressure measurements can be performed with good accuracy when sailing in upwind conditions, which thus would allow the sail trim and the sail shape to be enhanced on-the-water, taking into account the dynamic effects neglected in wind-tunnel tests.

The good agreement between the numerical results and the wind tunnel tests shows that inviscid codes can predict pressure distributions on upwind sails with great accuracy on most of the sail sections. However, Viola et al., 2011a, showed that inviscid codes are unable to accurately compute the pressure distribution near the head of sails where the influence of the tip vortex is stronger, and the flow is very three-dimensional.

Downwind

The aerodynamic forces on the sails, rigging and hull computed with the Navier-Stokes solver were compared with the wind tunnel data. The experimental forces were measured with the balance placed below the model. The comparison between aerodynamic coefficients, defined as the forces non-dimensionalised by the reference dynamic pressure q_∞ and sail surface area, showed very good agreement. For instance, Table 2 gives the numerical and experimental drive and side force coefficients, *Cx* and *Cy*, and it can be seen that the differences are smaller than 0.5%.

Figure 8 shows *Cp* on three sections of the asymmetric spinnaker. While the numerically computed *Cp* are in very good agreement with the wind tunnel *Cp*, the latter and full-scale *Cp* show some similarities and some differences.

The full-scale *Cp* shows that the resulting trim was too tight. In fact, the secondary leeward local maximum pressure related to leading edge flow reattachment is absent, whereas it is evident at about 0.3 of the sail girth in the wind tunnel and CFD results. Conversely, in full-scale a high suction peak occurs at the leading edge in all three measurement locations. Interestingly a suction peak was

measured on the leeward side on the top section near the trailing edge. This result has never been observed nor in wind tunnel tests or in numerical simulations, to the knowledge of the authors, and remains unexplained. It could be related to the interaction of the asymmetric spinnaker with the mainsail or, more likely, to a local stable vortex with a significant reverse velocity at the trailing edge, due to too a tight trim. The symmetry of the pressure distribution also suggests that the top section of the asymmetric spinnaker could be acting like a delta wing, with separation occurring off both edges.

On the bottom section, the pressure plateau on the leeward side, from 60% of the sail girth to the trailing edge, shows evidence of trailing edge separation. Note that in downwind conditions the sails are trimmed to be near the maximum lift instead of being near the maximum lift/drag ratio as for upwind sailing conditions. Therefore a larger trailing edge separation region is to be expected.

In downwind conditions, three-dimensional effects are particularly important in determining the resulting pressure distributions. The camber of downwind sails can be about 30% of the section chord, and the AoA can be higher than 35°. 2D profiles with such high cambers and AoA would stall. Conversely, most of the horizontal sections of asymmetric spinnakers work below the stall angle but show trailing edge separation downstream of the second half of the girth due to their high curvature. For instance, Figure 9 shows numerical computations of streamlines ("constrained" to lie on the sail) on the two surfaces of the asymmetric spinnaker. The flow on the windward side (left) has a significant vertical component: the flow above the clew height tends to go up, while the flow below the clew height tends to go down to the foot of the sail. The flow on the leeward side (centre) is almost horizontal in the attached region. Separated flow is shown in a thin region near the leading edge (zoomed view on the right), and in a wider region near the trailing edge.

The leading edge bubble was modelled properly by the numerical simulation, which allowed good accuracy in the computation of the leading edge pressure recovery. In fact, Figure 8 shows good agreement in the local maximum *Cp* at about 7% of the sail girth in the mid-section. The leading edge bubble is also shown in Figure 9 (left) and Figure 10, which shows it on a mid-horizontal section of the spinnaker. Velocity vectors are coloured by the flow speed in m/s, while streamlines are coloured by the vertical component of the velocity in m/s. It can be seen that vertical velocity components inside the bubble are significant. Figure 11 shows a perspective view of the same section. While only the plan projection of the vector fields is presented, the three-dimensional streamlines are shown. The streamlines closest to the leading edge show a helicoidal path inside the leading edge bubble. Note that all the plotted streamlines are on the leeward side of the sail.

The more stable wind-tunnel conditions compared to full-scale, enabled a more eased trim to fly successfully. Moreover, aerodynamic forces, pressures and flying shapes were measured simultaneously, making the wind tunnel the ideal environment to enhance sail design. However, the full-scale tests allowed practical sail trims to be investigated, which resulted in more tightened trims than in the wind tunnel, due to the various perturbations related to the real gusty wind, waves, etc., which tend to collapse the spinnaker in full-scale if it is not trimmed in hard enough. As for the results from sailing upwind, it is evident that the full-scale downwind pressure measurements allow the sail trim and the sail shape to be enhanced. However, the repeatability and accuracy of such downwind measurements is significantly affected by the associated more unsteady sailing conditions.

Navier-Stokes simulations provide a huge amount of additional information. In fact, the forces and the pressures on the sails are computed, as well as the velocity and pressure fields in the entire computational domain. The present paper shows that very high accuracy can be achieved with little

computational resources and time. While different sail trims are more easily and efficiently tested in the wind tunnel, sail design modifications can be tested very efficiently with CFD. For instance, the effect of lengthening the top section chord of the spinnaker can be more easily investigated with a new CFD simulation than by building a new sail and performing an additional wind tunnel test. Moreover, the high repeatability of CFD simulations allows systematic variation of a sail design parameter to be investigated and the trends on aerodynamic performance obtained.

CONCLUSIONS

It is common practice to investigate sail aerodynamics with any of three methods: full-scale tests, wind-tunnel tests and computational fluid dynamics. In particular, full-scale tests are mostly performed by comparing the performance of two (almost identical) boats, wind tunnel tests are mostly used to measure aerodynamic forces, and numerical methods are used to compute the pressure distribution on sails. In the last five years, the growth of new technologies has increased the interest in full-scale and wind-tunnel pressure measurements. In the present paper, the results of a two-year project aimed at comparing pressure distributions obtained with the three methods are presented. In particular, the pressure distributions on three horizontal sections of upwind and downwind sails are presented.

The difficulties and the advantages of each method are discussed. In addition, the similarities and the differences between the pressure distributions achieved with the three methods are debated.

In general good agreement was found between the pressure distributions achieved with the three methods. In particular, pressures computed numerically were in very good agreement with pressures computed in the wind tunnel. Conversely, downwind full-scale measurements showed the largest disagreement, due to the more tightened sail trim used in full-scale to keep the spinnaker from collapsing in the unsteady natural sailing conditions resulting from the gusty wind and the associated waves.

Full-Scale Testing

Full-scale testing takes into account the dynamic effects due to wind oscillations, yacht movements, course corrections applied by the helmsman, and the consequent sail trim variations. These effects resulted in a more tightened trim of the asymmetric spinnaker compared to the optimum trim measured in the wind tunnel.

In upwind conditions, the full-scale tests enabled pressures to be measured during periods of small sail trim and course alterations, resulting in relatively good repeatability. Conversely, very low test repeatability and accuracy was found in the downwind conditions due to the more unsteady nature of the test environment.

In both upwind and downwind full-scale measurements, the pressure distributions were found to be a useful tool to help understand sail aerodynamics, and to improve the sail trim or the sail shape. The authors believe that pressure measurements can be used onboard in real-time to significantly improve sail trim, and to provide the sail designer with useful suggestions for improving the sail design.

Wind-Tunnel Testing

The wind-tunnel tests allowed testing in a stable and controlled environment. Pressure measurements, forces, and flying shapes were measured simultaneously. The flexible sails allowed the sail trim to be modified as easily as in full-scale. Therefore, the effects of a sail trim variation on the pressures and on

the resulting aerodynamic forces can be efficiently investigated in the wind tunnel.

Wind tunnel pressure measurements were performed with both rigid sails and flexible sails. The two techniques were both effective. While the flexible sails allowed the sail trim to be changed as easily as in full-scale, the rigid sails allowed better control of the sail shape and thus better test repeatability.

Numerical Analysis

The upwind wind-tunnel test was modelled with a Vortex Lattice code. The computed pressure distributions on the three sail sections in general showed very good agreement with the corresponding upwind experimental results, thus showing that potential flow codes can be used effectively to improve sail design in upwind conditions. However, the numerical/experimental agreement decreased on the highest sail sections due to the significant viscous effects at the head of the sails, which are neglected by potential flow codes, thus pointing out their limitations.

The wind-tunnel downwind test was modelled with a Navier-Stokes numerical code. The forces and the pressure distributions computed by the code were in good agreement with the experimental data. In particular, differences in the lift and drag were smaller than 0.5%. The numerical analysis also provided a wide range of additional data. For instance, the velocity and the pressure fields were computed over the range of few boat lengths from the yacht. Importantly, these computations did not require large computational resources and large amounts of time.

Therefore numerical analysis can be very efficient for specific investigations. For instance, small changes in sail design can be more easily tested by modifying a numerical model than by building a new full-scale or model-scale sail. Conversely, the sail trim is more easily modified with a physical sail than numerically. Thus overall, it is clear from the results presented in this paper that each of the three methods to determine pressure distributions over sails has its advantages and disadvantages, and the designer/researcher needs to select the appropriate technique depending upon the questions to be answered.

ACKNOWLEDGMENTS

The authors wish to acknowledge the support of staff and students in the Yacht Research Unit, and in particular, the authors are grateful to Mr Julien Pilate who wrote and ran the Vortex Lattice code, and Mr Baptiste Watier and Mr Etienne Gauvain for the passion and the support in managing and performing the on-water and wind tunnel experiments. The authors also acknowledge the support of Dr Nick Velychko in building and supporting the multi-channel pressure system. The authors acknowledge the many useful discussions and sage advice from Mr David Le Pelley.

REFERENCES

Flay R.G.J., 1996. A Twisted Flow Wind Tunnel for Testing Yacht Sails. *Journal of Wind Engineering and Industrial Aerodynamics*, vol. 63, pp. 171-182

Flay R.G.J. & Millar S., 2006. Experimental Consideration Concerning Measurements in Sails: Wind Tunnel and Full Scale. *In the proceedings of the 2nd High Performance Yacht Design Conference (HPYDC2)*, pp. 123-130, 14th-16th February, Auckland, New Zealand.

Fossati F., Muggiasca S., Viola I.M., Zasso A., 2006. Wind Tunnel Techniques for Investigation and Optimization of Sailing Yachts Aerodynamics. *In the proceedings of the 2nd High Performance Yacht Design Conference (HPYD2),* pp. 105-113, 14th-16th February, Auckland, New Zealand.

Gentry A.E., 1971. The Aerodynamics of Sail Interaction. *In the proceedings of the 3rd AIAA Symposium on the Aero/Hydronautics of Sailing*, Redondo Beach, California, USA.

Gentry A.E., 1988. The Application of Computational Fluid Dynamics to Sails. *In proceedings of the Symposium on Hydrodynamic Performance Enhancement for Marine Applications*, Newport, Rhode Island, USA.

Graf K. & Mueller O., 2005. Der Twist-Flow-Windkanal der Yacht Research Unit Kiel. *In the proceedings of The 25th Symposium Yacht Design and Yacht Construction*, November, Hamburg, Germany.

Hansen H., Jackson P.S. and Hochkirch K., 2003. Real-Time Velocity Prediction Program for Wind Tunnel Testing of Sailing Yachts. In the proceedings of *In The Modern Yacht Conference, RINA*, Southampton, UK.

Hedges K.L., Richards P.J., Mallison G.D., 1996. Computer Modelling of Downwind Sails. *Journal of Wind Engineering and Industrial Aerodynamics*, vol. 63, pp. 95-110.

Hochkirch K. & Brandt H., 1999. Full-Scale Hydrodynamic Force Measurement on the Berlin Sailing Dynamometer. *In the proceedings of The 14th Chesapeake Sailing Yacht Symposium (14CSYS), SNAME,* pp. 33-44, 30th January, Annapolis, Maryland, USA.

Masuyama Y. & Fukasawa T., 1997. Full-Scale Measurements of Sail force and Validation of Numerical Calculation Method. *In the proceedings of The 13th Chesapeake Sailing Yacht Symposium (13CSYS), SNAME,* pp. 23-36, 25th January, Annapolis, Maryland, USA.

Milgram J.H., 1968a. The Aeodynamics of Sails. *In the proceedings of the 7th Symposium of Naval Hydrodynamics*, pp. 1397-1434.

Milgram J.H., 1968b. The Analytical Design of Yacht Sails. *In the SNAME annual meeting*, pp. 118-160.

Milgram J.H., Peters D.B., Eckhouse D.N., 1993. Modeling IACC Sail Forces by Combining Measurements with CFD. *In the proceedings of The 11th Chesapeake Sailing Yacht Symposium (11CSYS), SNAME*, pp. 65-73, 29th-30th January, Annapolis, Maryland, USA.

Miyata H., Lee Y.W., 1999. Application of CFD Simulation to the Design of Sails. Journal of Marine Science and Technology, vol. 4, pp. 163-172.

Puddu P., Erriu N., Nurzia F., Pistidda A., Mura A., 2006. Full Scale Investigation of One-Design Class Catamaran Sails. *In the proceeding of The 2nd High Performance Yacht Design Conference (HPYDC2),* February 14th-16th, Auckland, New Zealand.

Renzsch H., Müller O. and Graf K., 2008. FLEXSAIL – A Fluid Structure Interaction Program for the

Investigation of Spinnakers. *In the proceedings of the International Conference on Innovations in High Performance Sailing Yachts*, Lorient, France

Richter H.J., Horrigan K.C., Braun J.B., 2003. Computational Fluid Dynamics for Downwind Sails. *In the proceedings of The 16th Chesapeake Sailing Yacht Symposium*, March, Annapolis, Maryland, USA

Rodi W. 1991. Experience with Two-Layer Models Combining the k-e Model with a One-Equation Model Near the Wall. *In the proceedings of The 29th Aerospace Sciences Meeting,* AIAA 91-0216, 7th-10th January, Reno, Nevada, USA.

Viola I.M., 2009. Downwind Sail Aerodynamics: a CFD Investigation with High Grid Resolution. *Ocean Engineering, vol. 36, issues 12-13,* pp. 974-984.

Viola I.M. & Flay R.G.J., 2009. Force and Pressure Investigation of Modern Asymmetric Spinnakers, *International Journal of Small Craft Technology, Trans. RINA*, vol. 151, part B2, pp. 31-40.
Discussion in *Trans. RINA*, vol. 152, part B1, pp. 51-53.

Viola I.M. & Flay R.G.J., 2010a. Full-scale Pressure Measurements on a Sparkman and Stephens 24-foot Sailing Yacht, *Wind Engineering and Industrial Aerodynamics*, vol. 98, pp. 800–807.

Viola I.M. & Flay R.G.J., 2010b. Pressure Distribution on Modern Asymmetric Spinnakers, *International Journal of Small Craft Technology, Trans. RINA,* vol. 152, part B1, pp. 41-50.

Viola I.M. & Flay R.G.J., 2010c On-Water Pressure Measurements on a Modern Asymmetric Spinnaker. *In the proceedings of The 21th International HISWA Symposium on Yacht Design and Construction*, 15th-16th November, Amsterdam, Netherlands.

Viola I.M., Pilate J., Flay R.G.J., 2011a. Upwind Sail Aerodynamics: a Pressure Distribution Database for the Validation of Numerical Codes, *International Journal of Small Craft Technology*, *Trans. RINA,* vol. 153, part B1, pp. 47-58.

Viola I.M. & Flay R.G.J., 2011b. Sail Aerodynamics: Understanding Pressure Distributions on Upwind Sails, *Experimental Thermal and Fluid Science*, in press. DOI: 10.1016/j.expthermflusci.2011.06.009

Warner E.P. & Ober S., 1925. The aerodynamics of Yacht Sails, *in the proceedings of The 3rd General Meeting of the Society of Naval Architects and Marine Engineers,* 12th-13th November, New York, USA.

Werner, S., 2001. Application of the vortex lattice method to yacht sails, *Master of Engineering Thesis,* The University of Auckland, New Zealand.

Wilkinson S., 1984. Partially Separated Flows Around 2D Masts and Sails, *PhD Thesis,* University of Southampton, UK.

Zasso A., Fossati F., Viola I.M., 2005. Twisted Flow Wind Tunnel Design for Testing Yacht Sails. In proceedings of *The 4th European and African Conference on Wind Engineering (EACWE4),* Praga, Ceca Republic.

Table 1: Summary of sources of additional information

	Numerical	Wind-tunnel	On-water
Upwind	Viola et al., 2011a	Viola et al., 2011b	Viola et al., 2010a
Downwind	Present paper	Viola et al., 2009 Viola et al., 2010b	Viola et al., 2010c

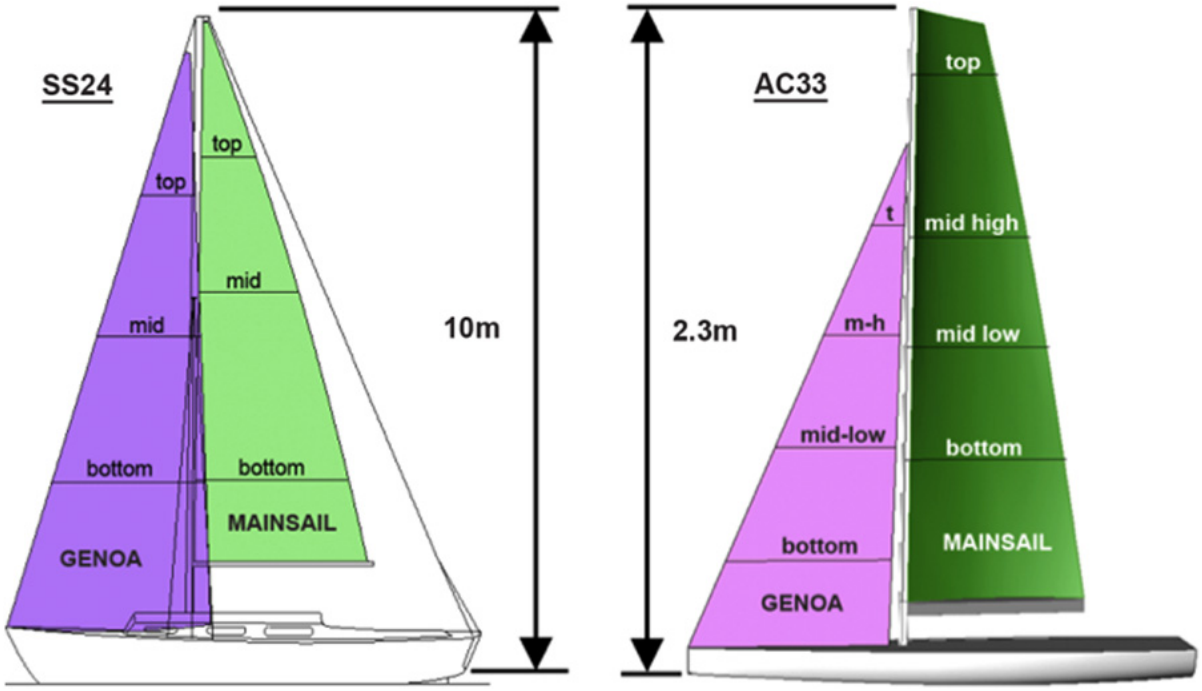

Figure 1: Sailplan of the model-scale AC33-class yacht and the yacht Aurelie.

Figure 2: Downwind sailing configurations for the pressure measurements: on-water (Platu-25 left) and wind tunnel (right). In the full-scale tests, the mainsail was reefed slightly in order to align the top of the spinnaker and mainsail to the same height

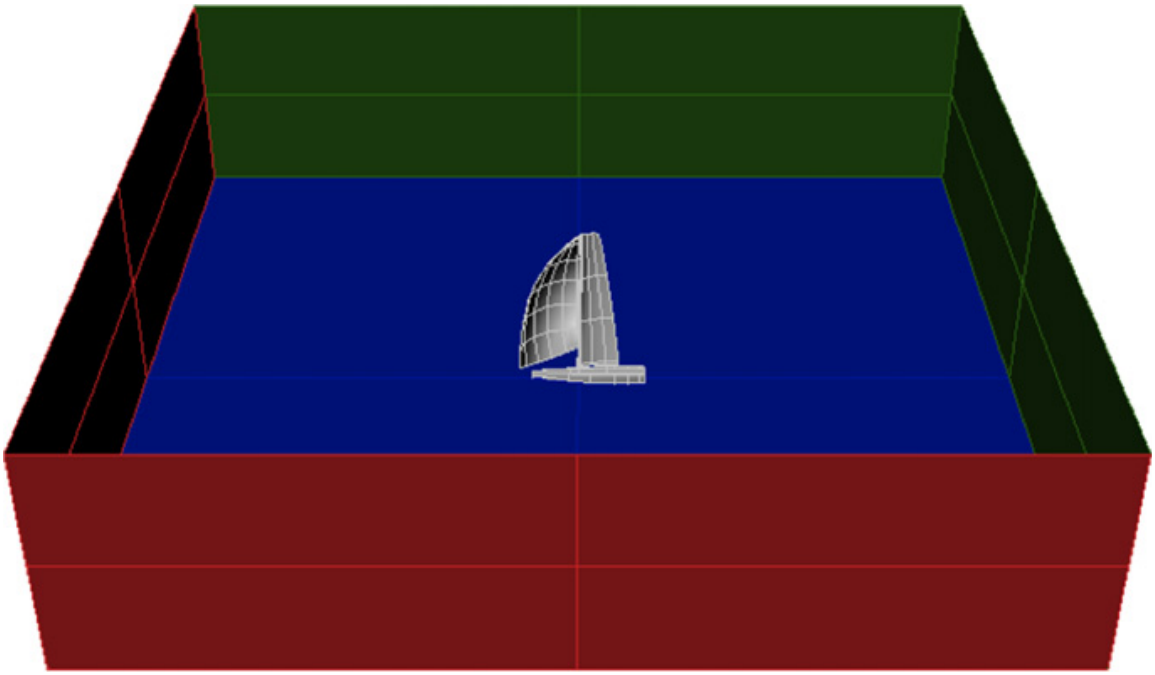

Figure 3: Computational domain.

Figure 4: Grid resolution.

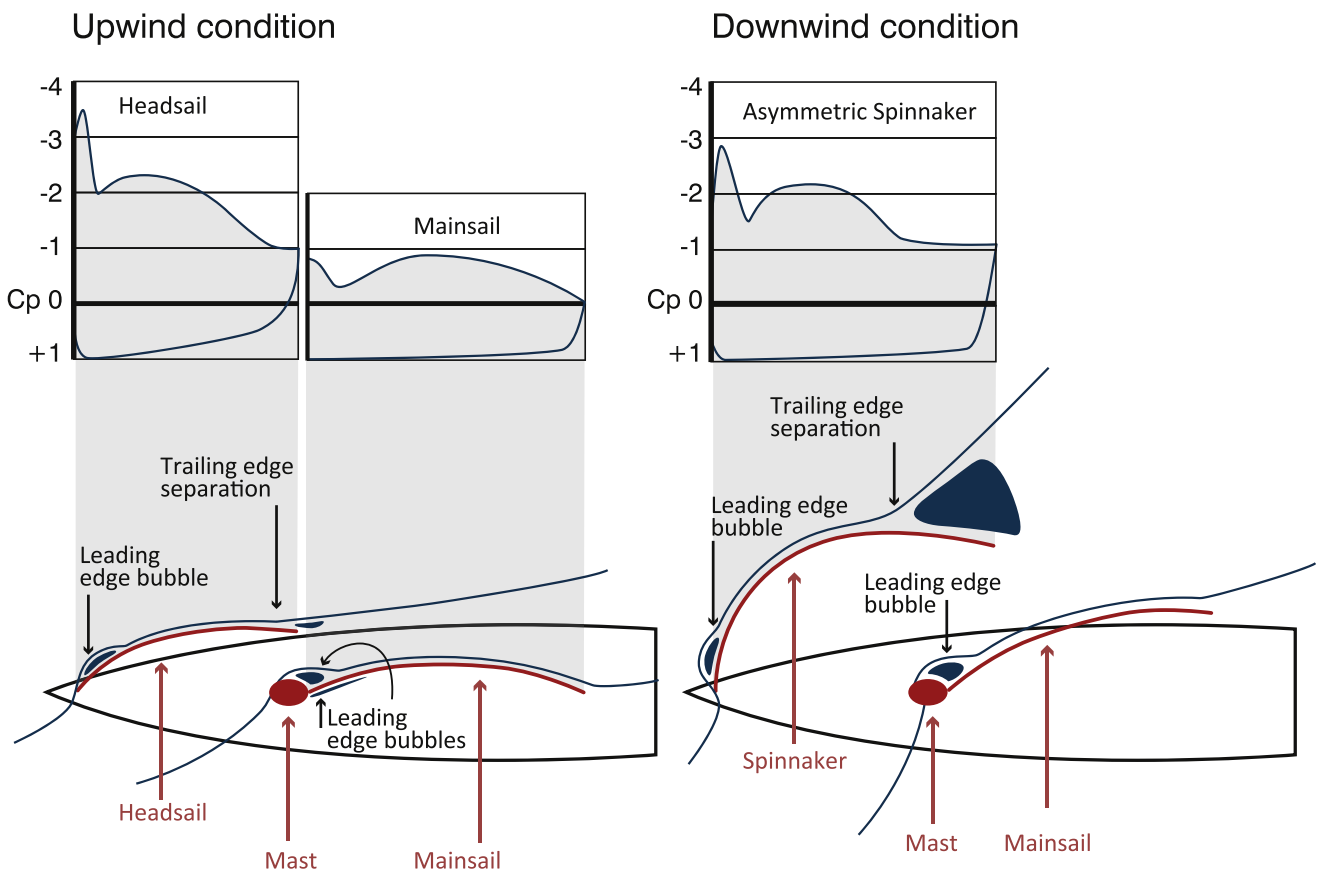

Figure 5: Schematic drawing of the flow and pressures around the sails.

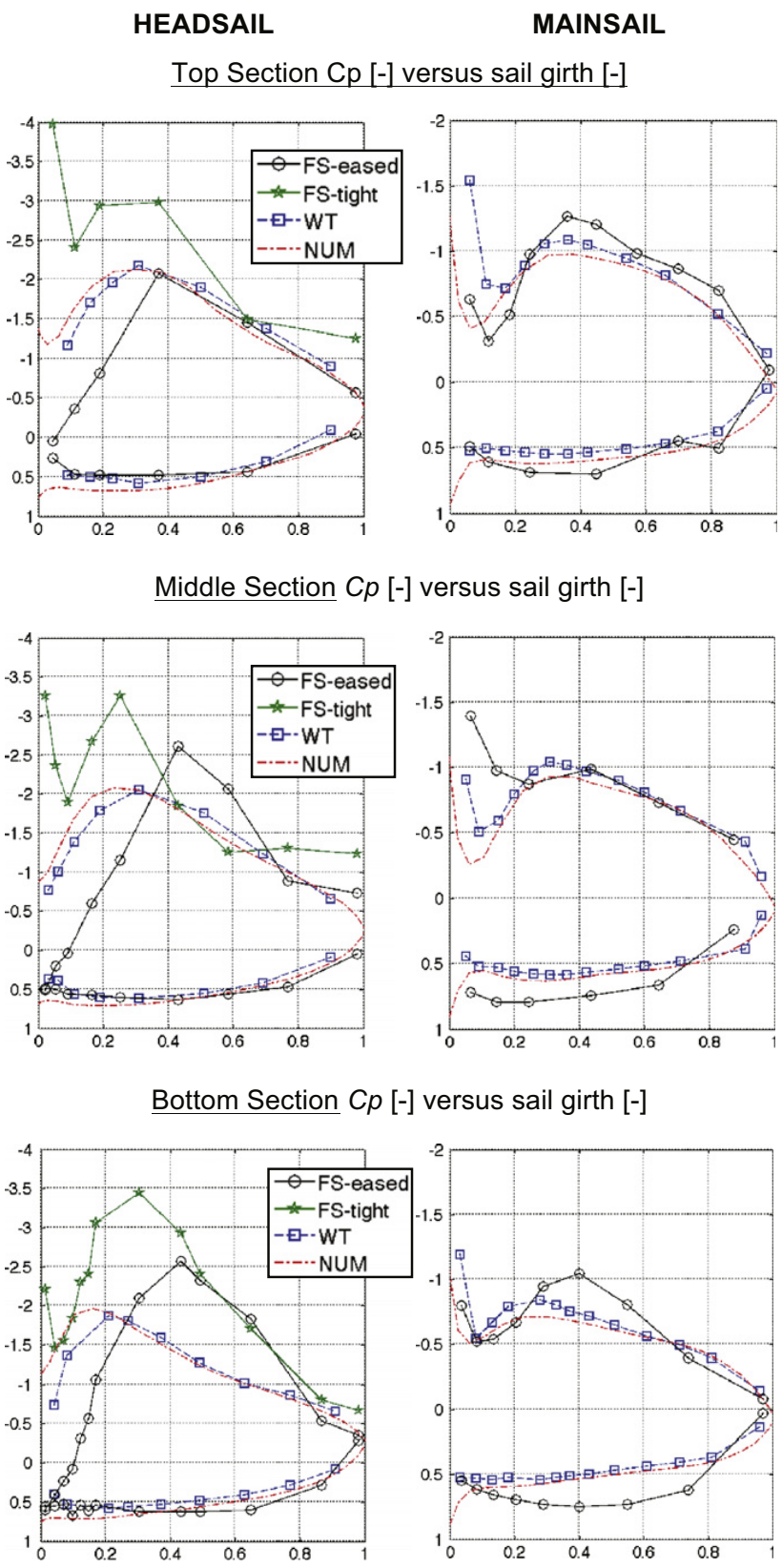

Figure 6: Full-scale (S&S24-class yacht), wind-tunnel (AC33-class yacht) and numerical (AC33-class yacht) *Cp* versus normalised sail girth for three horizontal sections of headsail and mainsail in upwind conditions.

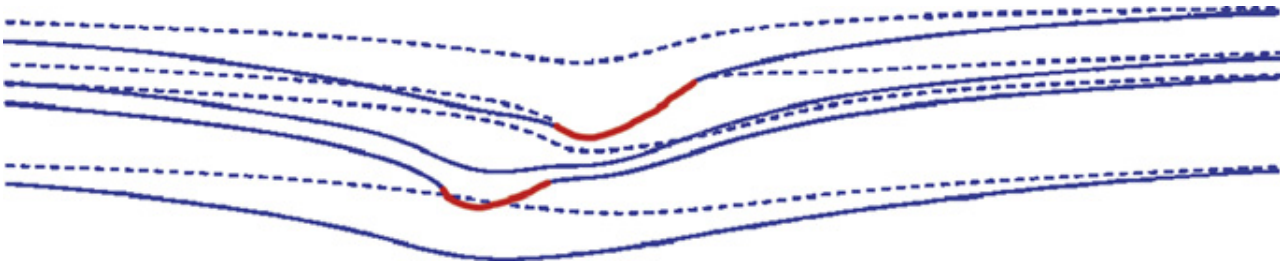

Figure 7: Streamlines with and without the headsail. Solid lines – headsail and mainsail present, dotted lines – mainsail alone.

Table 2: *Cx* and *Cy* from CFD and experiment.

	CFD	**WT**	**Difference**
Cx	0.871	0.869	0.24%
Cy	1.384	1.389	0.33%

ASYMMETRIC SPINNAKER

Top Section *Cp* [-] versus sail girth [-]

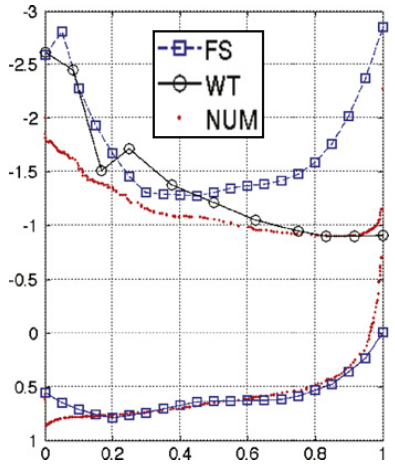

Middle Section *Cp* [-] versus sail girth [-]

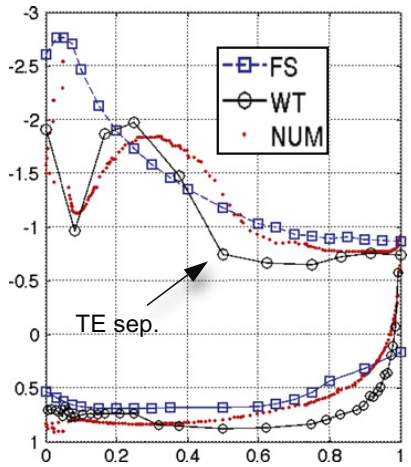

Bottom Section *Cp* [-] versus sail girth [-]

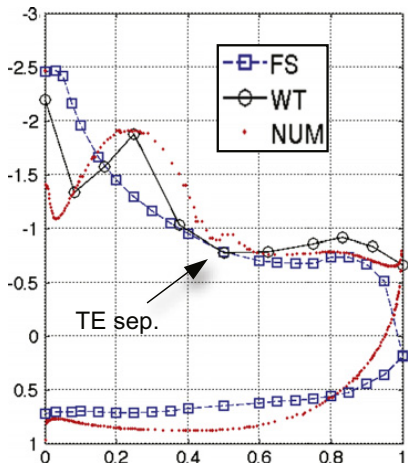

Figure 8: Full-scale, wind-tunnel and numerical *Cp* versus sail girth.

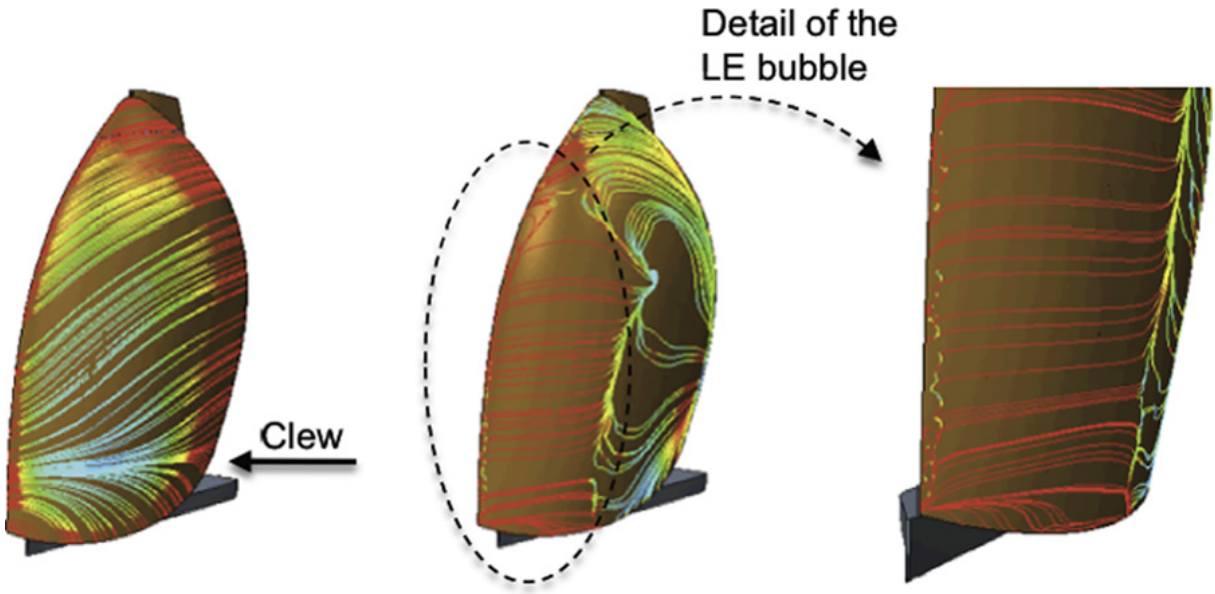

Figure 9: Numerical computations of the streamlines on the windward (left) and leeward (centre & right) sides of the spinnaker.

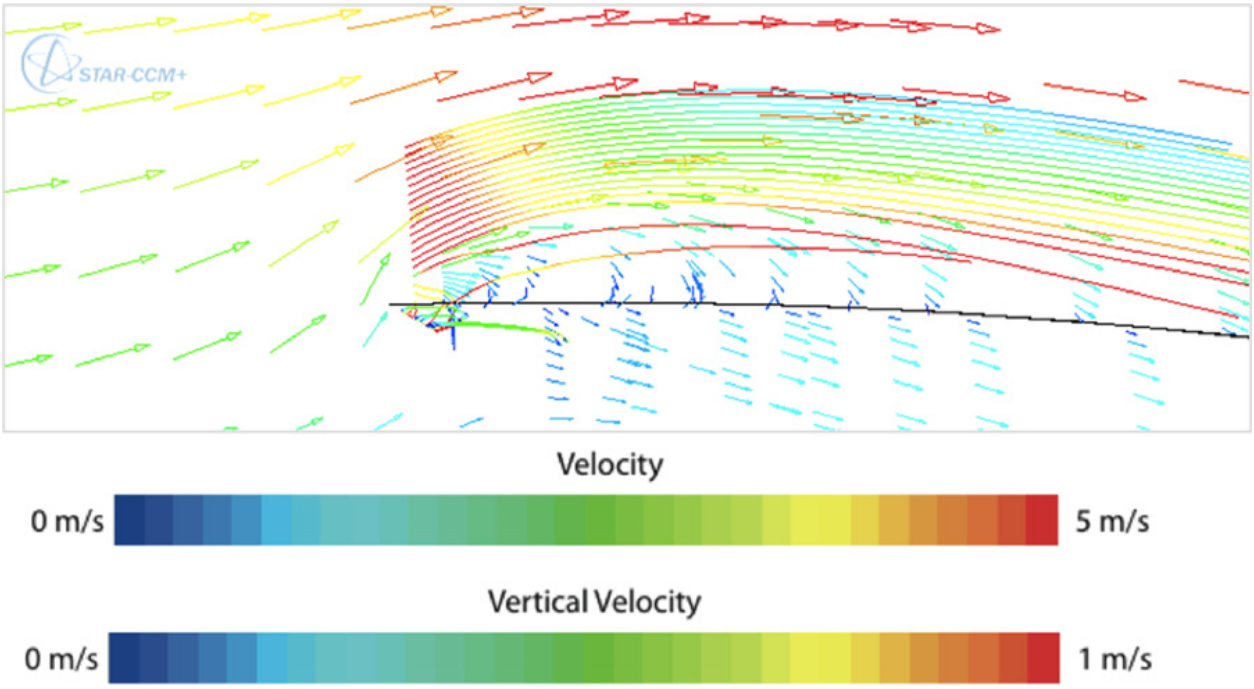

Figure 10: Leading edge bubble, plan view, from numerical computation.

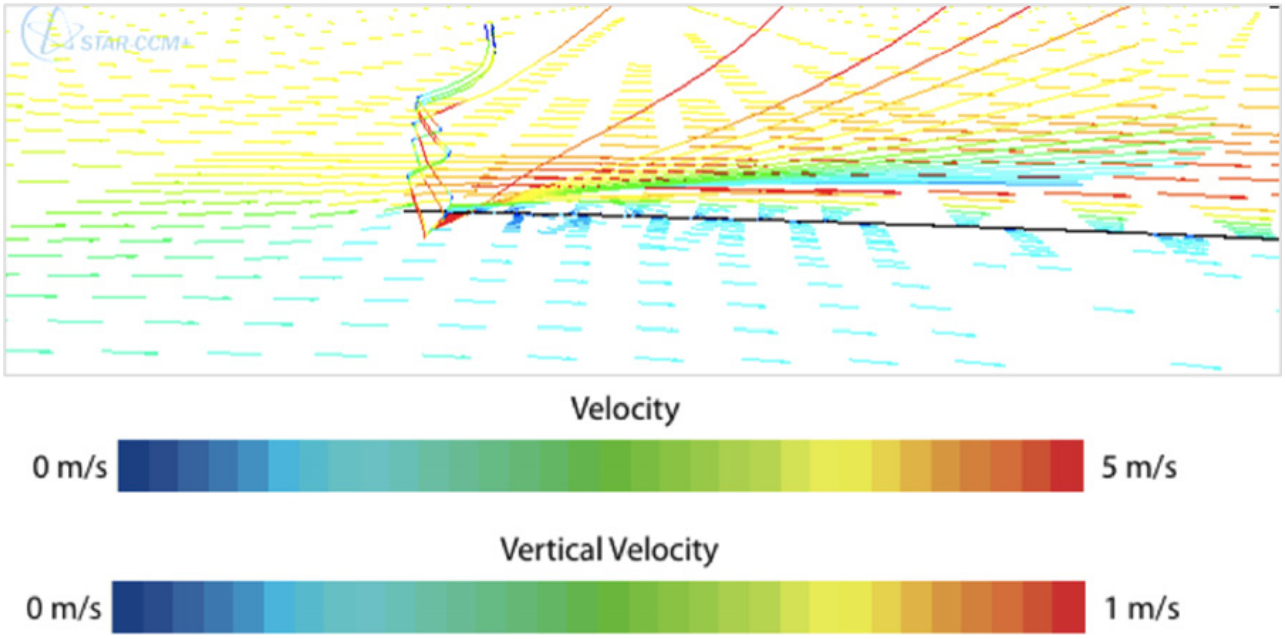

Figure 11: Leading edge bubble, perspective view, from numerical computation.